Article

In Situ Electrodeposited Synthesis of Electrochemiluminescent Ag Nanoclusters as Signal Probe for Ultrasensitive Detection of Cyclin-D1 from Cancer Cells

Ying Zhou, Maoxin Chen, Ying Zhuo, Yaqin Chai, Wenju Xu, and Ruo Yuan

Anal. Chem., **Just Accepted Manuscript** • Publication Date (Web): 01 Jun 2017

In Situ Electrodeposited Synthesis of Electrochemiluminescent Ag Nanoclusters as Signal Probe for Ultrasensitive Detection of Cyclin-D1 from Cancer Cells

Ying Zhou, Maoxin Chen, Ying Zhuo, Yaqin Chai, Wenju Xu*, Ruo Yuan*

Key Laboratory of Luminescent and Real-Time Analytical Chemistry (Southwest University), Ministry of Education, College of Chemistry and Chemical Engineering, Southwest University, Chongqing 400715, PR China

*Corresponding authors at: Tel.: +86 23 68252277, fax: +86 23 68253172.
E-mail addresses: xwju@swu.edu.cn (W. Xu); yuanruo@swu.edu.cn (R. Yuan).

ABSTRACT:

Metal nanoclusters (NCs) as a new type of electrochemiluminescence (ECL) nanomaterials have attracted great attention but their applications are limited due to relative low luminescent efficiency and complex preparation process. Herein, an ultrasensitive ECL biosensor for the detection of Cyclin-D1 (CCND1) was designed by utilizing in situ electrogenerated AgNCs as ECL emitters and Fe_3O_4-CeO_2 nanocomposites as coreaction accelerator. The ECL luminous efficiency of AgNCs on the electrode could be significantly enhanced with the use of the Fe_3O_4-CeO_2 for accelerating the reduction of $S_2O_8^{2-}$ to generate the strong oxidizing intermediate radical $SO_4^{\bullet-}$. As a result, the assay for CCND1 detection achieved excellent sensitivity with a linear range from 50 fg/mL to 50 ng/mL and limit of detection down to 28 fg/mL. Impressively, the efficiency of Traditional Chinese Medicines (TCM) - sophorae toward MCF-7 cell was successfully investigated due to the overexpression of CCND1 relation to the growth and metastasis of MCF-7 human breast cancer cell. In general, the proposed strategy provided an effective method for anticancer drug screening, and expanded the application of metal NCs in ultrasensitive biodetection.

KEYWORDS: electrochemiluminescence; electrodeposition; Ag nanoclusters; sophorae; anticancer drug screening

INTRODUCTION:

Cancer has become the first killer of human life and health throughout the world, what is more, cancer incidence has been rising fast in the developing countries owing to the aggravation of environment pollution, the acceleration of the aging process, and the universal existence of unhealthy lifestyle. [1-3] Traditional Chinese Medicines (TCMs) as the significant experience-based remedy have been derived from hundreds or thousands of years of clinical use in China, in which many herbs have provided a

simple, efficient, and economical drug therapy in the early stage cancer. [4-6] For instance, sophorae, which is the extractive of legume radix, may release an integrated anti-tumor ingredient through multiple targets associated molecular pathways. However, sophorae was not widely recognized as an efficient anticancer drug due to its lack of experimentally testable efficiency. Recent investigations indicated that Cyclin-D1 (CCND1), a kind of overexpression protein in MCF-7 human breast cancer cell, could be used as an excellent tumor marker for malignant degree of cancer cell. [7-9] Thus CCND1 with high affinity were labeled with signal molecule to act as detection probes for cells apoptosis monitoring. Inspired by these, an electrochemiluminescence (ECL) biosensor was first designed for anticancer sophorae screening through quantitative determination of protein expression.

Since Ras et al. explored ECL properties of silver nanoclusters (AgNCs) in 2009, [10] AgNCs have received widespread interest due to their dramatically different optical, electrical and chemical properties owning to the strong quantum confinement of electrons in the ultrasmall size regime. [11-13] In general, AgNCs have been synthesized through reducing Ag ions in aqueous solution, but it easily results in large nanoparticles rather than small AgNCs due to the aggregation tendency of AgNCs. [14, 15] Therefore, it is necessary to seek a simple, fast and controllable preparation strategy of AgNCs. In this work, AgNCs with glycine as the stabilizer were first synthesized by one-step electrochemical process in $LiClO_4$-glycine buffer containing 1 mM $AgClO_4$. Based on the capability of glycine to in situ sequester Ag ions, Ag ions can be reduced to Ag atoms and then Ag atoms aggregate into AgNCs on the electrode surface. [16, 17] Compared with reported NCs in solution, the proposed AgNCs were directly electrodeposited on the electrode, meanwhile, the size and structure of the AgNCs could be easily controlled by optimizing electrodeposition conditions.

As a novel ECL luminophore, the AgNCs have plentiful fascinating features, such as low toxicity, easy labeling, and excellent stability. [18-20] However, the luminous intensity of metal NCs remained too low to achieve sensitive biodetection. Recently, we employed cytosine-rich DNA as ligands to electrochemically generate AgNCs on the electrode as ECL signal probes for sensitive detection of microRNA with the promotion of $S_2O_8^{2-}$. [21] But the work suffered from the problem of harsh operating condition of DNA. Furthermore, the improvement of the ECL performance of AgNCs was limited due to lack of effective catalytic strategy. Amazingly, some nanoparticle or micromolecule as the co-reaction accelerator could effectively promote the reduction of co-reactant to generate stronger oxidizing intermediate radical, which would significantly amplify the ECL signal of luminophore in the coreactant path of ECL emission. [22] Magnetic Fe_3O_4 nanoparticles (NPs) have been used widely in biological sample extraction, targeted drug delivery, and magnetic resonance imaging. [23-25] Meanwhile, it was reported that Fe_3O_4 NPs in the size regime from tens of nanometers to submicrometers possessed an intrinsic enzyme-mimicking activity toward peroxide. [26, 27] In the work, the Fe_3O_4-CeO_2 nanocomposites were employed to improve ECL performance of AgNCs/$S_2O_8^{2-}$ system, in which reversible and rapid switching of the redox pair Ce^{3+}/Ce^{4+} could enhance the catalytic activity of the nanocomposites. (The electrochemical properties of CeO_2 and Fe_3O_4-CeO_2 was added in the supporting information.) As expected, the Fe_3O_4-CeO_2 as the co-reaction accelerator effectively promoted the reduction of $S_2O_8^{2-}$ to generate the strong oxidizing intermediate radical $SO_4^{\bullet-}$, which could react with AgNCs to produce excited state species AgNCs* for emitting ECL remarkably.

Inspire of these advantages, the AgNCs-based ECL biosensor was constructed for screening sophorae efficiency based on the Fe_3O_4-CeO_2 nanocomposites as the

catalytic probe and CCND1 protein expression as the evaluation factor. Initially, the AgNCs were electrodeposited on the sensing interface to act as signal probes, which could be used to immobilize anti-CCND1 *via* Ag-N or Ag-S bond. Subsequently, the Fe_3O_4-CeO_2-PtNPs nanocomposites were synthesized for capturing target protein (CCND1) from MCF-7 cell treated with sophorae. Based on the double-antibody sandwich of protein recognition, the exporting protein was quantified to demonstrate the anticancer efficiency of sophorae. The responses of the ECL biosensor would be decreased with increasing concentration of sophorae, because the less ratio of CCND1 were captured on the sensing surface and less Fe_3O_4-CeO_2-PtNPs/anti-CCND1 probes were combined on CCND1. Inspired by the intellectual scientific interests, the strategy initiated a new thought to anticancer drug screen, and paved the way for metal NCs in ultrasensitive biodetection and clinical diagnosis.

EXPERIMENTAL SECTION

Cell Culture. The MCF-7 human breast cancer cell line was obtained from the cell bank of the Committee on Type Culture Collection of Chinese Academy of Science (Shanghai, China). According to the manufacturer's instructions, the MCF-7 cells were cultured in100 U/mL streptomycin, DMEM/F-12 containing 10% FBS, and 100 U/mL penicillin and maintained in a humidified atmosphere with 5% CO_2 at 37 ºC. The live MCF-7 cells were respectively treated with sophorae concentrations of 0.5 mg/mL, 1.0 mg/mL, 1.5 mg/mL, 2.0 mg/mL, and blank for 24 h.

Preparation of the Fe_3O_4-CeO_2-PtNPs Labeled Anti-CCND1. Initially, the Fe_3O_4-CeO_2-PtNPs nanocomposites were prepared according to the hydrothermal method (the detailed synthetic process presented in Supporting Information). And then 1 mL prepared nanocomposites and 100 μL anti-CCND1 (secondary antibody, Ab_2) solution were added simultaneously in 900 μL PBS (pH 7.4) containing 400 mg

EDC and 100 mg NHS to synthesize Fe_3O_4-CeO_2-PtNPs/Ab_2 bioconjugates *via* Pt-S or Pt-N bond linking between Ab_2 and PtNPs. Subsequently, 200 μL bovine serum albumin (BSA, *w/w*, 1%) was implemented to block the unmodified portion of the Fe_3O_4-CeO_2-PtNPs surface in the reaction time of 40 min. Finally, the nanocomposites were removed and washed by magnetic separation, and then dispersed in 1.0 mL PBS solution (pH 7.4) to obtain Fe_3O_4-CeO_2-PtNPs/Ab_2/BSA probe. And the prepared process was shown in Scheme 1 A.

Fabrication of the Biosensor's Sensing Interface. For in situ electrodeposited synthesis of AgNCs on glassy carbon electrode (GCE), we employed glycine to act as stabilizer of AgNCs. The conductive solution, consisting of 1 mM $AgClO_4$ in 2 mL $LiClO_4$-glycine buffer (pH = 6.86, 0.1 M $LiClO_4$ and 0.5 M glycine), was deaerated by bubbling nitrogen for about 15 min, keeping an inert atmosphere during the whole process. Then the AgNCs were electrodeposited on the potential cycling between 0 and 1.2 V at the scan rate of 0.05 V/s for 300 s with a constant temperature of 25 $^{\circ}$C. Then, 5 μL anti-CCND1 (primary antibody, Ab_1) was incubated on the AgNCs modified GCE for 8 h *via* Ag-N or Ag-S bond. Finally, Ab_1/AgNCs/GCE was immersed in PBS containing 1% BSA to block the nonspecific sites. (Cyclic voltammograms of in situ AgNCs generation on GCE were showed in the supporting information.)

Measurement Procedure. For detection, the CCND1 proteins from treated MCF-7 cells were captured by the Fe_3O_4-CeO_2-PtNPs/Ab_2/BSA probe. And then the resultant biosensor was incubated in the PBS containing Fe_3O_4-CeO_2-PtNPs/Ab_2/ BSA/CCND1 at 37 $^{\circ}$C for 30 min. Every resultant electrode was washed with PBS after each step to avoid physical absorption. Finally, the ECL intensity of the biosensor was investigated with a model MPI-E II multifunctional electrochemical

and chemiluminescent analytical system at room temperature. The fabrication and reacted mechanism of the biosensor was shown in Scheme 1.

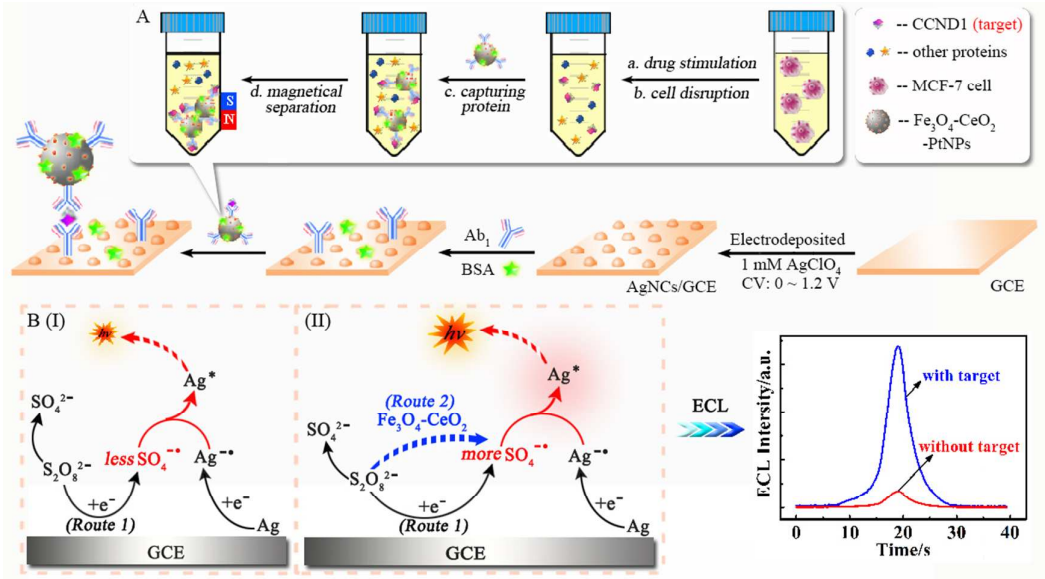

Scheme 1. The schematic diagrams showed fabrication of the ECL biosensor, (A) the process of capturing target CCND1 protein from the treated MCF-7 cell. (B) ECL mechanism of AgNCs/$S_2O_8^{2-}$ without (I) and with (II) the promotion of Fe_3O_4-CeO_2.

RESULTS AND DISCUSSION

TEM Characterization of Fe_3O_4-CeO_2-PtNPs. The stepwise formation of Fe_3O_4-CeO_2-PtNPs was confirmed using transmission electron microscope (TEM). Figure 1A was a typical TEM image of Fe_3O_4 NPs, which showed uniform sphere with an average size of 240 nm. While CeO_2 NPs were in situ synthesized around Fe_3O_4 NPs core, Figure 1B (Fe_3O_4-CeO_2) showed larger sphere with average size of 266 nm. Finally, Fe_3O_4-CeO_2-PtNPs nanocomposites (Figure 1C) presented homogeneous diameters of about 300 nm. And the amplified TEM image revealed that a large number of tiny Pt nanoparticles (PtNPs) assembled around Fe_3O_4-CeO_2 core. And X-ray photoelectron spectroscopy (XPS shown in the supporting information) was used for elemental analysis to further confirm preparion of the Fe_3O_4-CeO_2-PtNPs.

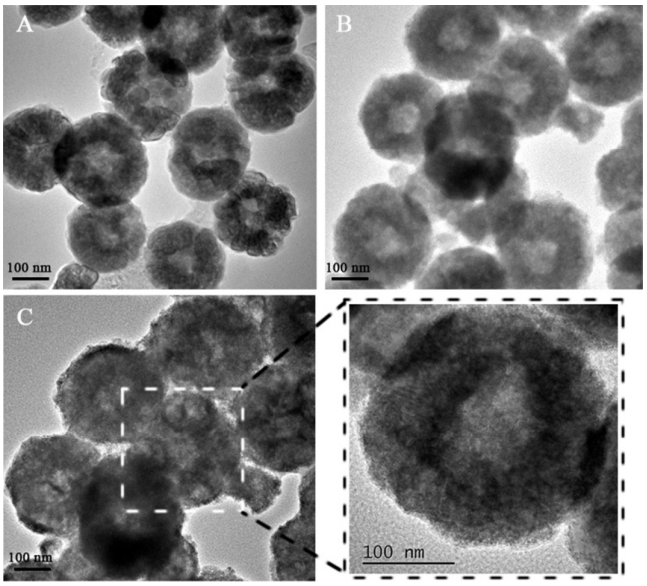

Figure 1. TEM images of Fe_3O_4 (A), Fe_3O_4-CeO_2 (B) and Fe_3O_4-CeO_2-PtNPs (C).

Morphology, Photophysical Characterizations of Electrogenerated AgNCs. The field emission scanning electron microscopy (FE-SEM) image (Figure 2A) indicated that the AgNCs consisted of a large number of nanospheres with an average particle size of 2.0 nm (the inset of Figure 2A). The diameter of AgNCs could be seen more clearly from the TEM image (Figure 2B). To investigate the crystal structure, the selected area electron diffraction (SAED) pattern, HRTEM and X-ray diffraction (XRD) pattern were recorded and showed in Figure 2C, 2D and 2E. The SAED pattern (Figure 2C) showed that diffraction spots were regularly arranged, indicating the monocrystalline structure of the nanoclusters. A series of 2D lattice fringes (Figure 2D) were examined to be 0.144 nm, which was similar to the (220) lattice spacing of the face-centered cubic (fcc) silver. [28] Furthermore, a typical X-ray diffraction (XRD) pattern was displayed in Figure 2E, and the peaks were correspondingly assigned to the diffraction of (111), (200), (220), (311) and (222) planes of fcc silver [29]. Finally, the ECL spectrum of AgNCs was measured by employing optical filters (spaced 25 nm) in the 2 mL PBS (pH 7.4) containing 5 mM $S_2O_8^{2-}$ with the potential scan ranging from -2 V to 0 V at 100 mV/s, and a

distinguished ECL peak at about 458 nm was observed (Figure 2F), which was approximate to the fluorescence emission spectrum (450 nm). From the photos in the inset of Figure 2F, the AgNCs aqueous solution emitted a blue luminescence under UV irradiation. The as-prepared AgNCs showed an absolute photoluminescence quantum yield (PLQY) of 3.2%, and high efficiency of ECL (Φ_{ECL}) which exceeded reported AgNCs in solution (Table S1).

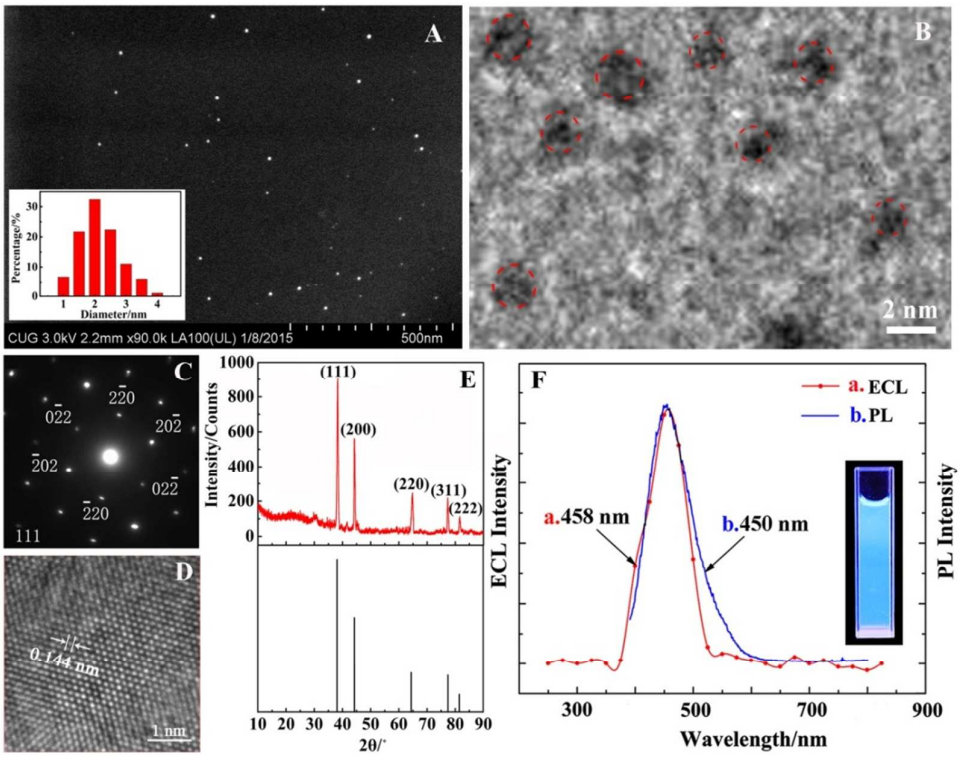

Figure 2. (A) FE-SEM images of the AgNCs, the insert of (A) : size distribution of the AgNCs determined from FE-SEM. **(B)** TEM image, **(C)** SAED **(D)** the amplified HRTEM image and (**E**) XRD pattern of AgNCs (upper plot) compared to a standard PDF card 04-0783 of Ag (lower plot). (**F**) The ECL spectrum (curve a) and the fluorescence emission (curve b) spectrum of AgNCs. The insert of (F) was photograph of AgNCs solution taken under UV light.

Possible ECL Emitting Mechanisms. ECL and CV measurements were implemented to validate the possible luminescent mechanism of AgNCs/$S_2O_8^{2-}$ system. As shown in Figure 3A, no distinct ECL emission could be observed from the bare GCE in PBS containing 5 mM $S_2O_8^{2-}$ (curve a), due to the lack of luminophor in

the system. When AgNCs modified GCE in the test solution, an obvious ECL response with the peak intensity of 1807 a.u. could be seen (curve b), declaring that the ECL emission indeed was produced by the excited state of AgNCs. Compared with the ECL of AgNCs/GCE, the Fe_3O_4-CeO_2/AgNCs/GCE showed higher ECL peak intensity at 6676 a.u, indicating that Fe_3O_4-CeO_2 could effectively improve ECL performance of AgNCs/$S_2O_8^{2-}$ system. (Comparison of catalytic activity of nanocomposites was showed in the supporting information.) Subsequently, the electrochemical property of Fe_3O_4-CeO_2 was investigated to explain the catalytic mechanism. From Figure 3B, bare GCE was measured in PBS containing 5 mM $S_2O_8^{2-}$, the reduction peak of $S_2O_8^{2-}$ was observed at −1.65 V (curve a), while the reduction peak of AgNCs was observed at −0.86 V (curve b) from AgNCs/GCE in PBS. Subsequently, the AgNCs/GCE was measured in PBS containing 5 mM $S_2O_8^{2-}$ (curve c), two reduction peaks could be observed at −0.86 V and −1.55 V, which respectively reflected the reduction reaction of AgNCs and $S_2O_8^{2-}$. While Fe_3O_4-CeO_2/AgNCs/GCE was detected, the CV curve (curve d) showed two more noticeable reduction peaks where the reduction potential shifted positively to −0.58 V and −1.39 V and the peak current increased apparently. These results showed that Fe_3O_4-CeO_2 as the co-reaction accelerator promoted the reduction of $S_2O_8^{2-}$ to generate the strong oxidizing intermediate radical ($SO_4^{\cdot-}$), and then $SO_4^{\cdot-}$ could in situ react with AgNCs to produce excited state species AgNCs* for emitting ECL remarkably.

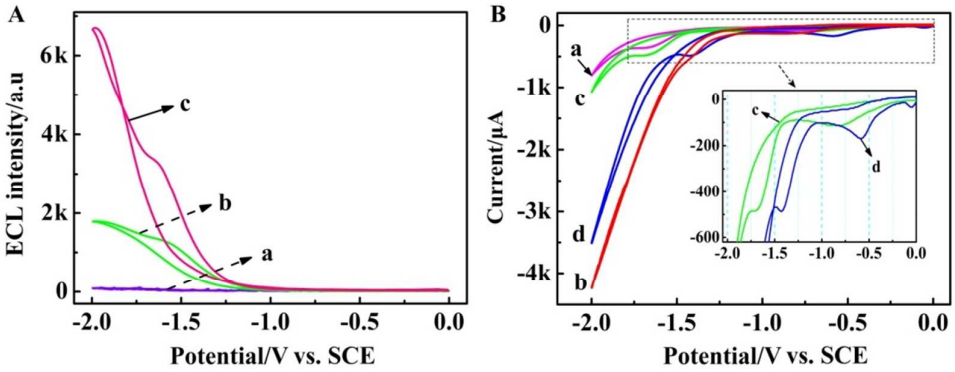

Figure 3. (A) ECL-potential curves of (a) bare GCE, (b) AgNCs/GCE and (c) Fe_3O_4-CeO_2/AgNCs/GCE in PBS containing 5 mM $S_2O_8^{2-}$. **(B)** Cyclic voltammograms of bare GCE (curve a), AgNCs/GCE (curve c) and Fe_3O_4-CeO_2/AgNCs/GCE (curve d) in PBS containing 5 mM $S_2O_8^{2-}$, and AgNCs/GCE in PBS (curve b), insert: the amplification of curve c and d.

But above all, under the catalysis of Fe_3O_4-CeO_2, $S_2O_8^{2-}$ was reduced to $S_2O_8^{\cdot 2-}$ (eq 2) and the AgNCs underwent a reduction reaction to negatively charged Ag radical ($Ag^{\cdot -}$, eq 1) in coreactant path. [30] Afterward, the strong oxidizing intermediate radical ($SO_4^{\cdot -}$) was generated through decomposition of $S_2O_8^{\cdot 2-}$ (eq 3), which accepted one electron from $Ag^{\cdot -}$ and transformed it to Ag* (eq 4). The Ag* excited state was generated by transferring one electron from $SO_4^{\cdot -}$ to the LUMO of Ag, which emitted intense light upon relaxation to the ground state (eq 5). The possible ECL mechanism was described as the following equations.

$$AgNCs + e^- \longrightarrow AgNCs^{\cdot -} \quad \text{.....[1]}$$

$$S_2O_8^{2-} + e^- \xrightarrow{Fe_3O_4\text{-}CeO_2} S_2O_8^{\cdot 2-} \quad \text{.....[2]}$$

$$S_2O_8^{\cdot 2-} \xrightarrow{Fe_3O_4\text{-}CeO_2} SO_4^{\cdot -} + SO_4^{2-} \quad \text{.....[3]}$$

$$SO_4^{\cdot -} + AgNCs^{\cdot -} \longrightarrow AgNCs^* + SO_4^{2-} \quad \text{.....[4]}$$

$$AgNCs^* \longrightarrow AgNCs + h\nu \quad \text{.....[5]}$$

Optimization of Electrodeposition Condition. To further explore ECL properties of electrogenerated AgNCs, we measured ECL responses of different sizes AgNCs, which were controlled by varying electrodeposition conditions such as the

electrodeposition solution and deposition time. First, electrodes were deposited in three kinds of electrodeposition solutions of (a) 1 mM $AgClO_4$ in $LiClO_4$-glycine buffer, (b) 1 mM $AgClO_4$ in 1-butyl-3-methylimidazolium tetrafluoroborate (BMT), and (c) 1 mM $AgClO_4$ in ultrapure water, respectively. As shown in Figure 4A, the highest ECL peak intensity (curve a) was achieved from the AgNCs, which was generated in the $LiClO_4$-glycine buffer. In the meantime, the FE-SEM image (Figure S5A) revealed that homogeneous and dispersive AgNCs with an average diameter of 2.0 nm could be generated in the $LiClO_4$-glycine buffer. Figure S5B showed that the AgNCs with larger size were synthesized in the BMT, while Figure S5C displayed that the AgNCs tended to reunite in ultrapure water. It indicated that glycine could control the nucleation and migration of reduced silver atoms. Similarly, the optimal deposition time was investigated, and the AgNCs with deposition time of 300 s could obtain the highest ECL emission (curve e, Figure 4B). Meanwhile, AgNCs with a homogeneous diameter of 2.0 nm were generated on GCE at 300 s (Figure S5E). Finally, the ECL properties of the AgNCs in the different concentration of $AgClO_4$ were investigated. The AgNCs generated in the 1 mM $AgClO_4$, not only exhibited the most remarkable cathodic ECL emission (curve g, Figure 4C), but also optimal morphology characterization (Figure S5G). Hence, control of the particle size and structure is a powerful strategy to modulate ECL properties of NCs.

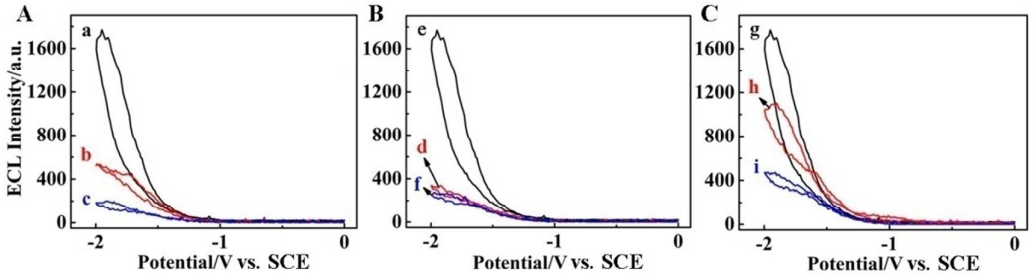

Figure 4. The ECL-potential curves (A) of different AgNCs/GCE by three kinds of electrodeposition solutions of 1 mM $AgClO_4$ in $LiClO_4$-glycine buffer (curve a), 1 mM $AgClO_4$ in

BMT (curve b), and 1 mM $AgClO_4$ in ultrapure water (curve c), respectively. The ECL-potential curves (B) of different AgNCs/GCE by different deposition time of 100 s (curve d), 300 s (curve e) and 500 s (curve f), respectively. The ECL-potential curves (C) of different AgNCs/GCE by different concentrations of $AgClO_4$ solutions, 1 mM $AgClO_4$ (curve g), 5 mM $AgClO_4$ (curve h), 10 mM $AgClO_4$ (curve i), respectively.

ECL Responses of the Biosensors toward CCND1. Under the optimal reaction conditions, the proposed biosensors were successively detected in 0.1 M PBS (pH 7.4) containing 5 mM $S_2O_8^{2-}$ by scanning the potential from 0 to −2.0 V at a scanning rate of 100 mV/s. As exhibited in Figure 5A, the ECL intensity increased with increasing concentration of CCND1 from 50 fg/mL to 50 ng/mL (curves a~h) and presented an excellent linear relationship with the logarithm of concentration. The linear equation was I = 1116 lg c + 5376 (where I was the ECL intensity and c was the CCND1 concentration). Moreover, the limit of detection was calculated to be 28 fg/mL according to three standard deviations of the blank responses. It was noticed that the proposed method showed prominent analytical performance of CCND1, which could be attributed to the excellent catalytic effect of Fe_3O_4-CeO_2 toward AgNCs/$S_2O_8^{2-}$ system. The comparison for existing NCs based bioanalysis demonstrated the prepared biosensor exhibited better sensitivity (Table 1).

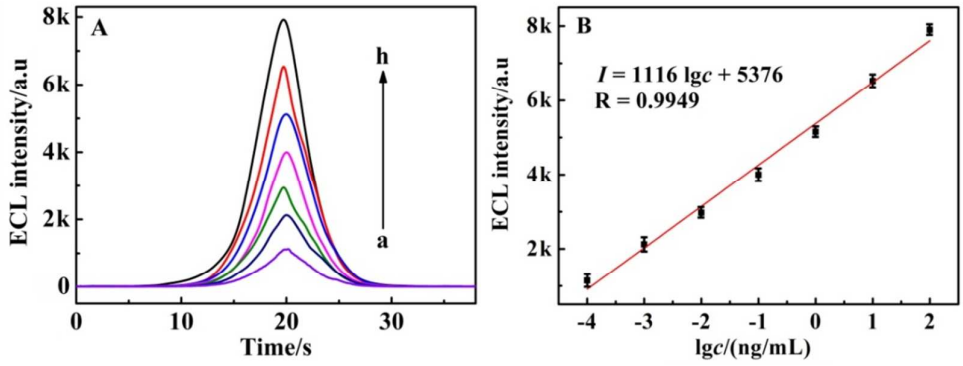

Figure 5. (A) ECL profiles of the biosensor incubating CCND1 with different concentrations: 50 fg mL^{-1}, 500 fg mL^{-1}, 5 pg mL^{-1}, 50 pg mL^{-1}, 500pg mL^{-1}, 5 ng mL^{-1}, 50 ng mL^{-1}, and 500 ng

mL^{-1}. (B) Calibration plots of the proposed biosensor.

Table 1. Comparison of this Work with the Previous Researches.

methods	signal probe	target	detection limit	references
fluorescence	AuNCs	human α -thrombin	36.7 μg mL^{-1}	31
fluorescence	AuNCs	histone deacetylase 1	175 ng mL^{-1}	32
electrochemistry	AgNCs	alpha-fetoprotein	0.8 pg mL^{-1}	33
photoelectrochemistry	AgNCs	carcinoembryonic antigen	1.0 pg mL^{-1}	34
ECL	PdNCs	carcinoembryonic antigen	0.62 pg mL^{-1}	35
ECL	AgNCs	CCND1	28 fg mL^{-1}	this work

Application of biosensor for Anticancer TCM Screening. To validate the performance of the proposed biosensor toward anticancer drug screening, the biosensor was employed to measure the CCND1 protein expression after MCF-7 cell treated with different doses of sophorae for 24 hour (Figure 6). When sophorae with higher concentration, the concentration of CCND1 from the treated MCF-7 cell reduced, less Fe_3O_4-CeO_2-PtNPs/Ab_2 probes could be immobilized on the biosensors, thus ECL responses of the proposed biosensors significantly decreased. Comparing with untreated cell (blank), the ECL signals of the proposed biosensor gradually decreased with augment of doses of sophorae (0.5 mg/mL, 1.0 mg/mL and 1.5 mg/mL), and the ECL signal dramatically declined when treated with a high dose of sophorae (2.0 mg/mL). It indicated that the proposed biosensor could be used for screening anticancer drug efficacy with cell apoptosis.

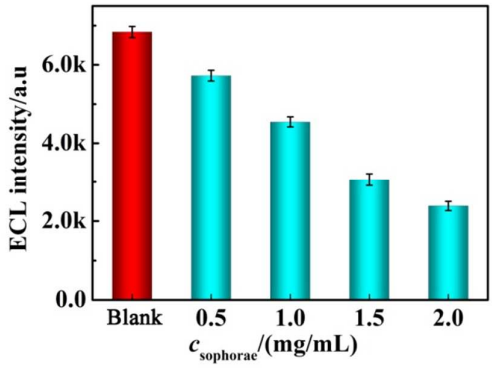

Figure 6. ECL signals of the biosensor incubated in the CCND1 from untreated cells and different treated cells.

Stability and Repeatability of the Proposed Biosensor. Stability as one of the important factors was investigated by employing the biosensor for consecutive cyclic potentials scans, which was evaluated for the proposed biosensor incubated with various concentration of CCND1 from the treated cell (Figure 7A). It could be found that relative stable curves could be obtained for the proposed biosensor on every concentration of CCND1, indicating the excellent stability of the biosensor. To further investigate the reproducibility, intra- and interassays were performed (Figure 7B), the relative standard deviations (ECL response) of intra- and interassays were 3.64% and 4.53%, respectively, which demonstrated an acceptable repeatability of the proposed biosensor for the application in anticancer drug screening.

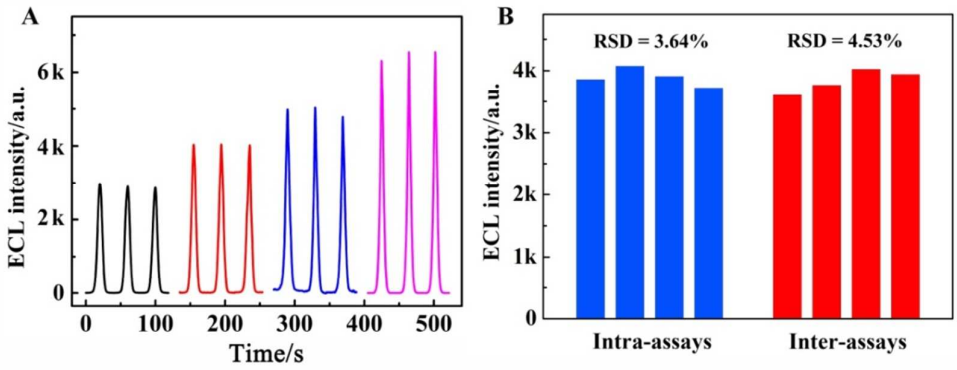

Figure 7. ECL stability (A) and reproducibility (B) of the proposed biosensor.

CONCLUSION

In this work, the in suit electrogenerated AgNCs based ECL biosensor for ultrasensitive detection of CCND1 was constructed to demonstrate the anticancer efficiency of sophorae owing to the high affinity of CCND1 to MCF-7 cell. Meanwhile, the Fe_3O_4-CeO_2 nanocomposites were employed as the coreaction accelerator to facilitate the reduction of $S_2O_8^{2-}$ for significantly promoting the ECL emission of AgNCs. Compared with the reported metal NCs based biosensor, the proposed biosensor not only had good response to CCND1 in a wide linear range with outstanding selectivity, but also provided a simple, fast and controllable preparation process of metal NCs. The study demonstrated the metal NCs integrated with quantitative protein expression monitoring could be open a new way for development of anticancer drug screening in the application of biomedicine and clinical diagnosis.

ASSOCIATED CONTENT

Supporting Information

Chemicals and apparatus, preparation of the Fe_3O_4-CeO_2-PtNPs, cyclic voltammograms of in situ AgNCs generation on glassy carbon electrode, XPS characterization of Fe_3O_4-CeO_2-PtNPs, comparison of ECL properties of AgNCs, the electrochemical properties of CeO_2 and Fe_3O_4-CeO_2, the FE-SEM micrograph of AgNCs by different electrodeposition conditions, comparison of catalytic activity of nanocomposites, electrochemical characterizations of the biosensor.

AUTHOR INFORMATION

* Corresponding authors

Tel.: +86 23 68252277, fax: +86 23 68253172.

E-mail addresses: xwju@swu.edu.cn (W. Xu), yuanruo@swu.edu.cn (R. Yuan).

Notes

The authors declare no competing financial interest.

ACKNOWLEDGMENT

This work was financially supported by the National Natural Science Foundation (NNSF) of China (Grants 21575116, 21675130 and 51473136) and the Fundamental Research Funds for the Central Universities (Grant XDJK2015A002), China.

REFERENCES

(1) Gelband, H.; Sankaranarayanan, R.; Gauvreau, C. L.; Horton, S.; Anderson, B. O.; Bray, F.; Cleary, J. *Lancet* **2016**, 387, 2133-2144.

(2) Cairns, R. A.; Mak, T. W. *Nat. Rer.* **2016**, 16, 613-614.

(3) Topalian, S. L.; Taube, J. M.; Anders, R. A.; Pardoll, D. M. *Nat. Rer.* **2016**, 16, 275-287.

(4) Fugh-Berman, A. *Lancet* **2000**, 355, 134-138.

(5) Zhou, H.; Sun, L.; Yang, X. L.; Schimmel, P. *Nature* **2013**, 494, 121-124.

(6) Normile, D. *Science* **2003**, 299, 188-190.

(7) Sicinski, P.; Donaher, J. L.; Parker, S. B.; Li, T.; Fazeli, A.; Gardner, H.; Haslam, S.; Bronson, F. T.; Elledge, S. J.; Weinberg, R. A. *Cell* **1995**, 82, 621-630.

(8) Lamb, J.; Ramaswamy, S.; Ford, H. L.; Contreras, B.; Martinez, R. V.; Kittrell, F. S.; Zahnow, C. A.; Patterson, N.; Golub, T. R.; Ewen, M. E. *Cell* **2003**, 114, 323-334.

(9) Aran, D.; Hellman, A. *Cell* **2013**, 154, 11-13.

(10) Díez, I.; Pusa, M.; Kulmala, S.; Jiang, H.; Walther, A.; Goldmann, A. S.; Müller, A. H. E.; Ikkala, O.; Ras, R. H. A. *Angew. Chem. Int. Ed.* **2009**, 48, 2122-2125.

(11) Javani, S.; Lorca, R.; Latorre, A.; Flors, C.; Cortajarena, A. L.; Somoza, A. *ACS Appl. Mater. Interfaces* **2016**, 8, 10147-10154.

(12) Jie, G. F.; Tan, L.; Zhao,Y.; Wang, X. C. *Biosens. Bioelectron.* **2017**, 94, 243-249.

(13) Zhang, L.; Zhu, J.; Zhou, Z.; Guo, S.; Li, J.; Dong, S.; Wang, E. *Chem. Sci.* **2013**, 4, 4004-4010.

(14) Yao, Q.; Yu, Y.; Yuan, X.; Yu, Y.; Zhao, D.; Xie, J.; Lee, J. Y. *Angew. Chem. Int. Ed.* **2015**, 54, 184-189.

(15) Xu, H. X.; Suslick, K. S. *ACS Nano* **2010**, 6, 3209-3214.

(16) Tian, N.; Zhou, Z. Y.; Yu, N. F.; Wang, L. Y.; Sun, S. G. *J. Am. Chem. Soc.* **2010**, 132, 7580-7581.

(17) Hines, T.; Díez-Perez, I.; Nakamura, H.; Shimazaki, T.; Asai, Y.; Tao, N. *J. Am. Chem. Soc.* **2013**, 135, 3319-3322.

(18) Liu, Y.; Ai, K.; Cheng, X.; Huo, L.; Lu, L. *Adv. Funct. Mater.* **2010**, 20, 951 -956**.**

(19) Wei, W.; Lu, Y.; Chen, W.; Chen, S. *J. Am. Chem. Soc.* **2011**, 133, 2060-2063**.**

(20) Hesari, M.; Workentin, M. S.; Ding, Z. *ACS Nano* **2014**, 8, 8543-8553**.**

(21) Chen, A. Y.; Ma, S.; Zhuo, Y.; Chai, Y. Q.; Yuan, R. *Anal. Chem.* **2016**, 88, 3203-3210.

(22) Ma, M. N.; Zhuo,Y.; Yuan, R.; Chai, Y. Q. *Anal. Chem.* **2015**, 87, 11389-11397.

(23) Zhang, W.; Zhang, Y.; Jiang, Q.; Zhao, W.; Yu, A.; Chang, H.; Lu, X.; Xie, F.; Ye, B.; Zhang, S. *Anal. Chem.* **2016**, 88, 10523-10532.

(24) Zhang, Y.; Hu, Z.; Qin, H.; Liu, F.; Cheng, K.; Wu, R.; Zou, H. *Anal. Chem.* **2013**, 85, 7038-7043.

(25) Liu, X.; Hui, J.; Jing, Y.; Gao, S.; Wu, C.; Li, C.; Li, J.; Wang, X. *Adv. Funct. Mater.* **2016**, 26, 8697-8706.

(26) Yang, S.; Cao, C.; Sun, Y.; Huang, P.; Wei, F.; Song, W. *Angew. Chem. Int. Ed.* **2015**, 54, 2661-2664.

(27) Zheng, T.; Zhang, Q.; Feng, S.; Zhu, J.-J.; Wang, Q.; Wang, H. *J. Am. Chem. Soc.* **2014**, 136, 2288-2291.

(28) Yu, D.; Yam, V. W.-W. *J. Am. Chem. Soc.* **2004**, 126, 13200-13201.

(29) Zhao, Y.; Kornienko, N.; Yang, P.; Yaghi, O. M. *J. Am. Chem. Soc.* **2015**, 137,

2199-2202.

(30) Ding, Z.; Quinn, B. M.; Haram, S. K.; Pell, L. E.; Korgel, B. A.; Bard, A. J. *Science* **2002**, 296, 1293-1297.

(31) Li, J.; Zhong, X.; Zhang, H.; Le, X. C.; Zhu, J. J. *Anal. Chem.* **2012**, 84, 5170-5174.

(32) Wen, Q.; Gu, Y.; Tang, L. J.; Yu, R. Q.; Jiang, J. H. *Anal. Chem.* **2013**, 85, 11681-11685.

(33) Zhang, B.; Liu, B.; Zhou, J.; Tang, J.; Tang, D. P. *ACS Appl. Mater. Interfaces* **2013**, 5, 4479-4485.

(34) Song, J.; Wang, J.; Wang, X.; Zhao, W.; Zhao, Y.; Wu, S.; Gao, Z.; Yuan, J.; Meng, C. *Biosens. Bioelectron.* **2016**, 80, 614-620.

(35) Huang, Y.; Lei, J.; Cheng, Y.; Ju, H. X. *Biosens. Bioelectron.* **2016**, 77, 733-739.

For TOC only

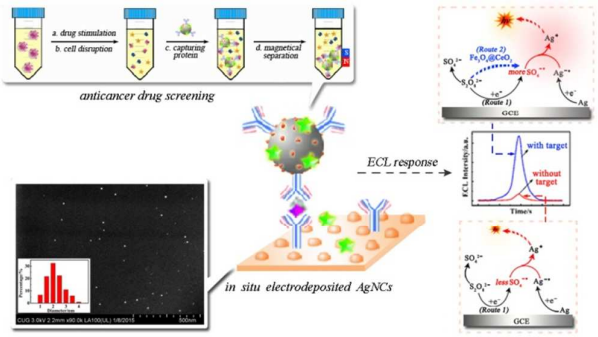
a. drug stimulation
b. cell disruption
c. capturing protein
d. magnetical separation
anticancer drug screening
ECL response
with target
without target
in situ electrodeposited AgNCs
GCE
(Route 1)
(Route 2)
more
less